12-1985

Characterization of Potassium Promoted & Unpromoted Fischer-Tropsch Catalysts

Steven Miller
Western Kentucky University

Miller,

Steven

1985

CHARACTERIZATION OF POTASSIUM PROMOTED AND UNPROMOTED FISCHER-TROPSCH CATALYSTS

A Thesis

Presented to

the Faculty of the Department of Chemistry

Western Kentucky University

Bowling Green, Kentucky

In Partial Fulfillment

of the Requirements for the Degree

Master of Science

by

Steven Miller

December 1985

AUTHORIZATION FOR USE OF THESIS

Permission is hereby

☑ granted to the Western Kentucky University Library to make, or allow to be made photocopies, microfilm or other copies of this thesis for appropriate research or scholarly purposes.

☐ reserved to the author for the making of any copies of this thesis except for brief sections for research or scholarly purposes.

Signed S R Mills

Date 10 February 1986

Please place an "X" in the appropriate box.

This form will be filed with the original of the thesis and will control future use of the thesis.

CHARACTERIZATION OF POTASSIUM PROMOTED AND UNPROMOTED FISCHER-TROPSCH CATALYSTS

RECOMMENDED August 1, 1985
(Date)

John M. Stencel
Director of Thesis

Lowell W. Shank

Gordon E. Sims Jr.

Approved January 3, 1986
(Date)

Edmund Gray
Dean of the Graduate College

TABLE OF CONTENTS

LIST OF TABLES

LIST OF FIGURES

CHARACTERIZATION OF POTASSIUM PROMOTED AND UNPROMOTED FISCHER-TROPSCH CATALYSTS

Steve Miller August 1985 52 pages

Directed by: John M. Stencel, Laurence J. Boucher, Lowell W. Shank, and Gordon Wilson, Jr.

Department of Chemistry Western Kentucky University

The technique of x-ray photoelectron spectroscopy (XPS) has been applied to characterize iron-manganese catalysts used in Fischer-Tropsch synthesis. The catalysts, which vary in composition from 10 FE/90 Mn, to 50 Fe/50 Mn are analyzed after being placed in a slurry reactor and having synthesis gas reacted over them. Changes in catalyst composition are investigated further using in situ techniques. Additionally, 20 Fe/80 Mn catalysts containing potassium in the range of 0.1 wt.% to 1.3 wt.% are analyzed in the same manner. These studies have permitted the identification of some of the factors influencing activation and deactivation, product selectivity, and surface speciation.

INTRODUCTION

The potential of using iron-manganese catalysts for the synthesis of olefin-rich hydrocarbons from coal-derived synthesis gas is of considerable interest because of the ease with which olefins can be upgraded to high quality transportation fuels or chemical feedstocks. In order to gain insight into the fundamental aspects of iron-manganese catalysts, a characterization study of some precipitated iron-manganese catalysts was undertaken using XPS (X-ray Photoemission Spectroscopy). The iron-manganese catalysts were reacted in an in situ reactor attached to the XPS spectrometer to determine the effect of activation sequences and conditions on the surface characteristics of the catalysts. To determine the effect of potassium promotion on these catalysts, potassium carbonate impregnated iron-manganese catalysts were investigated by XPS after reaction in a slurry reactor. These samples were also reacted in the in situ reactor to determine the potassium species present after exposure to Fischer-Tropsch synthesis conditions.

BACKGROUND

Fischer-Tropsch Synthesis

The Fischer-Tropsch (F-T) synthesis originated in Germany in the 1920's and reached its zenith during World War II where it provided motor fuels for the German Army.[1] Immediately after World War II, most industrial nations had F-T based projects in progress; and those were kept going briefly until cheap oil and gas made chemicals and fuels from coal non-competitive. At present, the F-T synthesis is nly utilized at a commercial scale only in the South African Sasol plants.

However, since the energy crisis of the early 1970's F-T synthesis has come under renewed attention as a production method of synthetic fuels and chemical feedstocks. The main factors behind this interest are rising energy and feedstock costs, decreased petroleum reserves, and sharply increased investment costs associated with tertiary recovery, off shore drilling, and deep gas wells. In addition, F-T synthesis has the potential of producing chemical feedstocks or motor fuels without the production of environmentally harmful compounds encountered in direct liquefaction of coal. The use of coal-derived synthesis gas overcomes most of these problems. More than 65% of the world's recoverable

fossil fuel reserves are coal while oil accounts for only 10%. In addition the U.S. has abundant coal reserves which could be used instead of imported oil as a base for transportation fuels and chemicals.

The classic F-T synthesis using cobalt or iron catalysts yields mainly saturated and unsaturated aliphatic hydrocarbons ranging from methane to high melting paraffins.[2] The main reaction of the F-T synthesis is[2,3]

$$CO + 2H_2 \longrightarrow (-CH_2-) + H_2O \qquad (1)$$

Water gas shift conversion (eq.2) occurs between the water formed and the CO of the synthesis gas.[1,2,3]

$$CO + H_2O \longrightarrow CO_2 + H_2 \qquad (2)$$

The net overall reaction can be summed as

$$2\,CO + H_2 \longrightarrow (-CH_2-) + CO_2 \qquad (3)$$

Undesirable side reactions that can complicate the synthesis include the Boudouard reaction

$$2\,CO \longrightarrow C + CO_2 \qquad (4)$$

coke disposition

$$H_2 + CO \longrightarrow C + H_2O \qquad (5)$$

and methanation

$$CO + 3H_2 \longleftrightarrow CH_4 + H_2O \qquad (6)$$

Additional oxidation of the catalyst and carbide formation

$$xM + yC \longrightarrow M_xC_y \qquad (7)$$

are also important in F-T synthesis.

In order to optimize product yields, the CO/H_2 ratio added must be the same CO/H_2 ratio consumed in the reaction.[1]

An excess of either gas, with respect to the other, will lead to a decreased product yield.

While several mechanisms have been proposed to explain the action of Fischer-Tropsch catalysts none are considered definitive. The three most commonly considered mechanisms[2] are

a) chain growth by condensation

b) chain growth by insertion of carbon monoxide into the metal-hydrocarbon bond

c) chain growth by polymerization of methylene groups

An example of chain growth by condensation is the Anderson-Emmett mechanism[3,4] which begins by formation of an enolic complex on the catalyst surface:

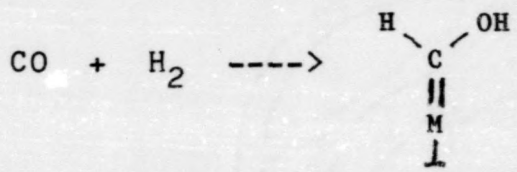

This is followed by the condensation of two M=CHOH groups followed by hydrogenation:

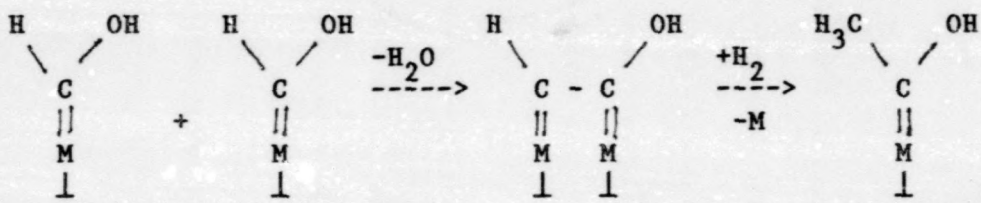

Further condensation and hydrogenation is then possible. Separation of the carbon from the metal during chain growth yields aldehydes, alcohols, acids, esters, olefins or saturated hydrocarbons.

According to the chain growth by insertion of carbon monoxide into the metal-hydrocarbon bond, which is typified by the Pichler mechanism,[3,5] the hydrocarbon chain starts with the formation of an aldehydic surface complex, which, by hydrogenation and dehydration, reacts via a methylene complex forming a methyl group.

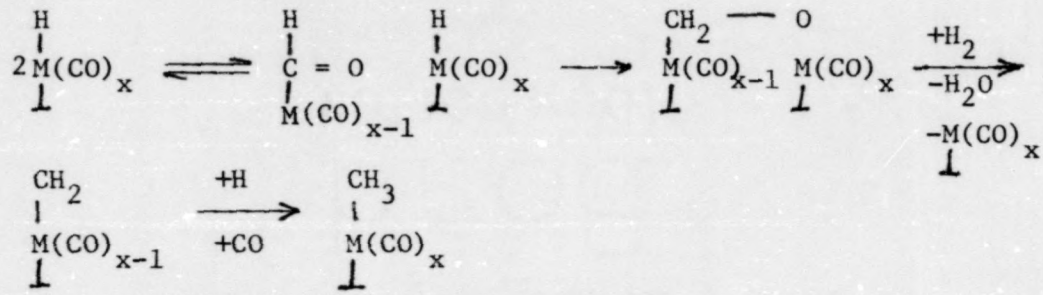

The methyl group may be converted by hydrogenation to methane or by insertion of a CO ligand between the metal-carbon bond to form a new aldehydic complex:

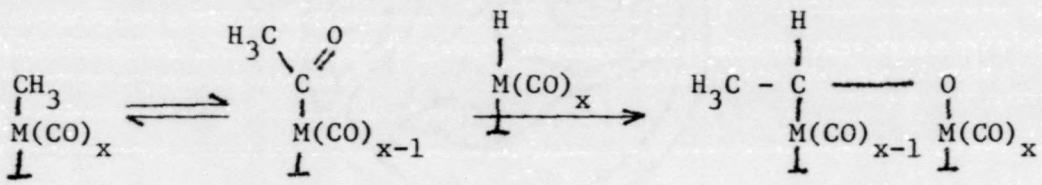

The carbon of this complex can then be lengthened by an alteration of hydrogenation, dehydration and CO insertion steps.

Chain growth by polymerization of methylene groups, was first suggested by Fischer and Tropsch. This mechanism involved the formation and hydrogenation of metal carbides to give methylene groups on the surface of the metal, which

then are polymerized and reacted further to give the observed products.(4)

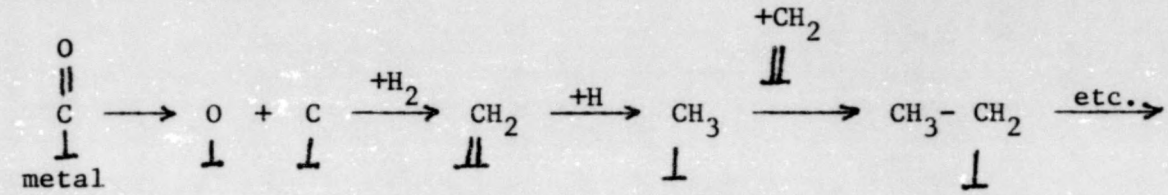

Each of these different methods has been supported or criticized by various investigators.(1-5) However, in each the overall reaction can be interpreted as being a sequence of the following steps:(2)

a) Chemisorption of CO and H_2 on the catalyst surface

b) Formation of a primary complex, after dissociation or weakening of the C-O bond and formation of a C-H bond.

c) Chain growth by interference of the primary complex with syngas or with product already formed and adsorbed

d) Chain termination, for example by hydrogenation or by reaction of the growing chain with synthesis products, followed by desorption from the surface.

Iron-Manganese Catalysts and Potassium Promotion

At present, the only operating F-T plants are in South Africa. Waxes, motor fuels, and pipeline gas are produced there. However, at today's market prices, naphtha substituted production via F-T synthesis appears to be economic under special conditions.(1) The direct synthesis of ethylene, propylene, and butene for chemical feedstocks

through F-T synthesis is more promising and requires a substantial improvement in the selectivity of the reaction leading to a preferred formation of lower olefins as primary products.[1,6,7]

To achieve this objective, new and more selective F-T catalysts have been proposed. Various researchers have found that iron-manganese catalysts offer improved selectivity for synthesis of C_2-C_4 Olefins.[6-7] Such catalysts, with a composition of 50Fe/50Mn weight percent with respect to iron, were reported to yield a product predominantly of C_2-C_4 light olefins, chain length of products extending only to about C_6, and methane formed in traces.[7,8] Different researchers have had less spectacular results.[9-12]

Another possibility of shifting the product distribution to the desired range is to add potassium promoters. These influence the basic metal electronically in the direction of improved selectivity.[2] Potassium salts have been used for this purpose successfully for decades. Contents of between 0.2 and 1.0 percent K_2CO_3, relative to iron, doubles the heat of CO chemisorption. Also the amount of adsorbed H_2 and its heat of chemisorption have been reported to decrease.[2,13-15] The consequences of this are

1. The velocities of CO consuming reactions - e.g. synthesis, conversion, and Boudouard reaction - increases.
2. Chain start and chain growth are accelerated.
3. The formation of methane is suppressed.
4. The olefin content of reaction products increases.

X-ray-Photoelectron Spectroscopy

The present work examines samples of promoted and non-promoted iron/manganese catalysts both before and after reaction with synthesis gas. These catalysts were characterized by X-ray photoelectron Spectroscopy (XPS). When a sample is bombarded by a photon (such as an X-ray) whose energy exceeds the binding energy of an electron in a given shell or subshell of an atom in the sample, there exists a finite probability that the incident photon will be absorbed by the atom and an atomic electron will be promoted to an unoccupied level or ejected completely as a photoelectron. The probability of photoelectron production depends on the energy of the incident photon and the atomic number of the target element.[14] To a first approximation the kinetic energy of the ejected photoelectron is given by the simple relationship

$$E_e = h_v - E_b$$

where E_e = kinetic energy of the photoelectron, h_v = the energy of the photon, and E_b = the binding energy of the electron in a given shell.

It is clear from the equation that if the incident photons are monoenergetic then the photoelectrons ejected from a given shell will also be monoenergetic. Thus the photoelectron spectrum of a material reflects the various occupied electronic levels and bands in the material. Further, because the binding energies are different for various elements, the photoelectron spectra are characteristic of the elements and can be used as the basis for identification. This is in fact the principle used in XPS. After the photoelectron is ejected from an atom, the atom is left in an excited state with an electron vacancy in one of the shells. There are two alternative ways for an atom to de-excite or to return to a lower energy state. One results in the emission of an Auger electron. The other results in the emission of a fluorescent X-ray.

These processes are summarized in Figure 1. On the left is the XPS process; the photon ejects a 1s electron from the atom. In the center diagram, an electron drops from the 2p orbital to fill the 1s hole, and a photon is emitted. This results in K X-ray emission. On the right-hand side, a 2s electron drops to fill the 1s hole, simultaneously expelling a 2p electron. This is called the KLL Auger process. Auger and X-ray emission are competitive processes.[17]

Figure 2 shows a block diagram of an X-ray photoelectron spectrometer. The spectrometer consists of an X-ray source, a sample, an electron energy analyzer, a

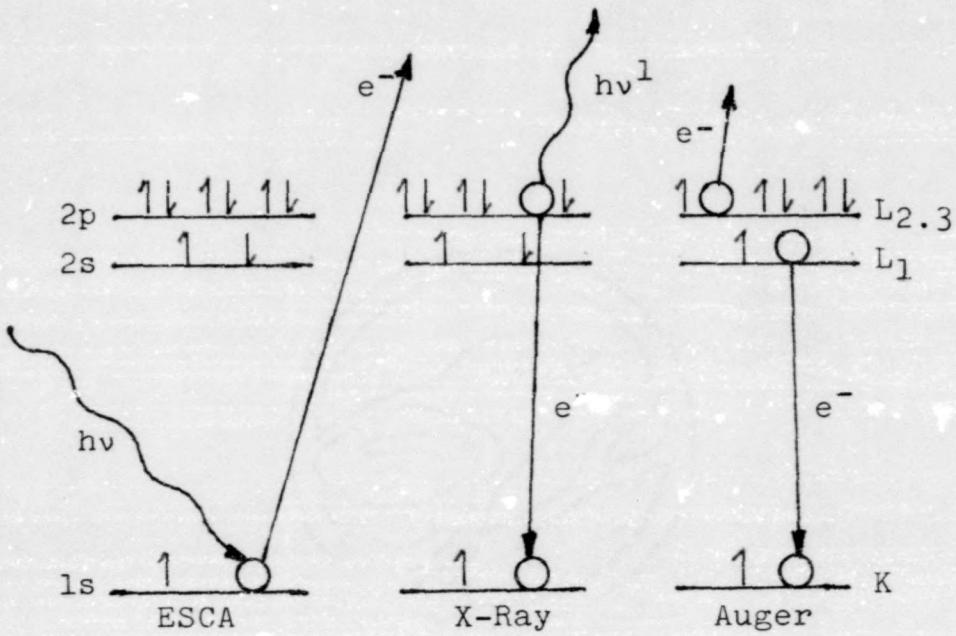

ENERGETICS

ESCA: $T_e = h\nu - E_B(1s)$

X-Ray: $H\nu^1 = E_B(1s) - E_B(2p)$

Auger: $T_e = E_B(1s) - E_B^1(2p)$

Figure 1. Diagram of ESCA, X-Ray, and Auger processes.[16]

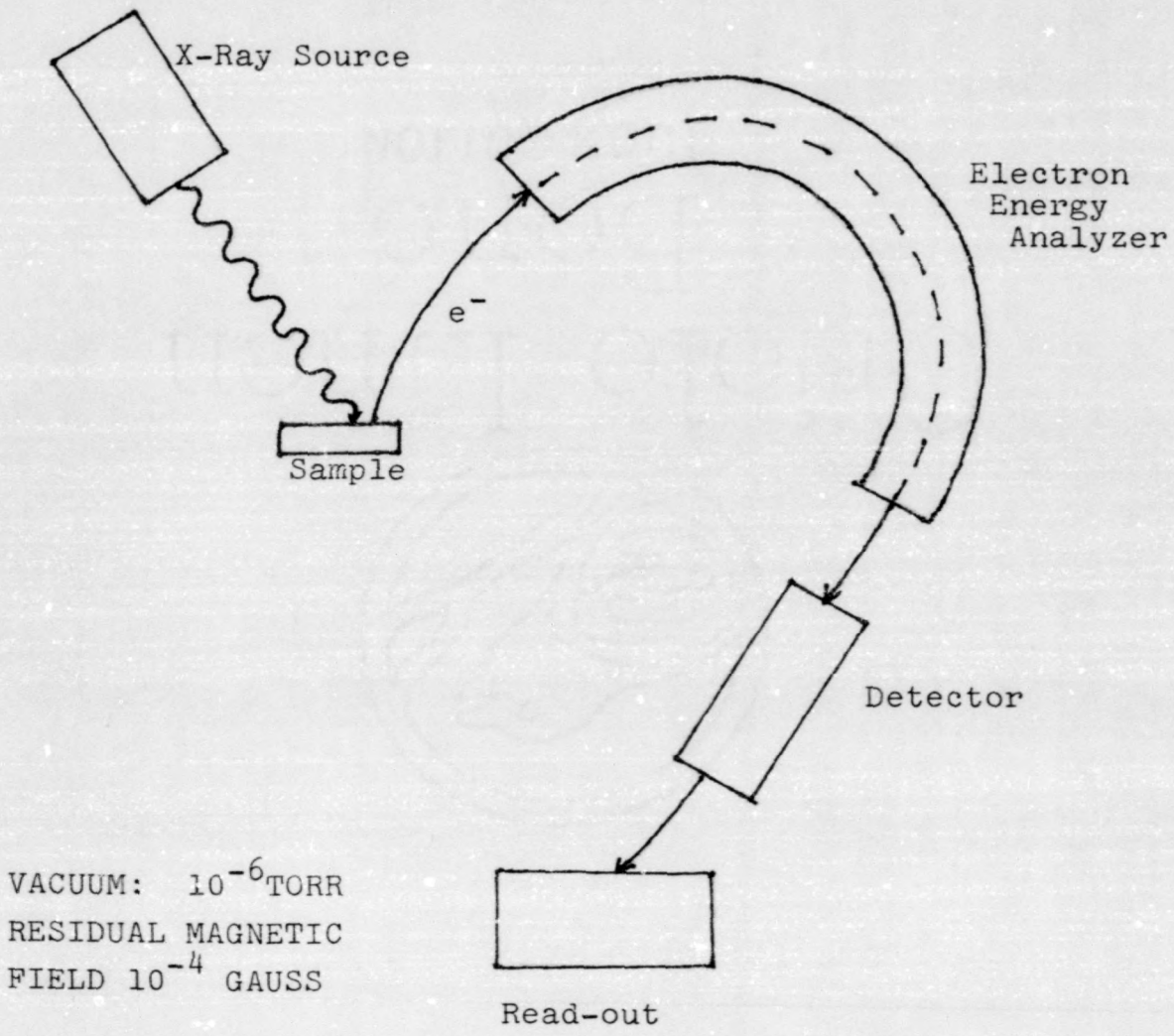

Figure 2. Block Diagram of Electron Spectrometer (2)

detector, and a read-out system. X-ray photoelectron spectrometers must operate under a vacuum of 10^{-6} torr or lower. At pressures higher than 10^{-6} torr, the interaction or scattering of electrons with residual gases in the chamber becomes excessive. Also, the residual magnetic field in the vicinity of the sample and analyzer must be reduced below 10^{-4} gauss. Stray magnetic fields can cause perturbation to the electron path and decreased electron transmission.(16)

The analytical characteristics of XPS are given in Table 1. Generally XPS electrons have kinetic energies of approximately 100-1500 eV with nominal escape depths of 10 A^{o}. The single most valuable attribute of XPS is its ability to provide information about chemical bonding (i.e., oxidation states of elements). It is sensitive to all elements except H and He. The specificity of XPS is very good, i.e., there is little systematic overlap of spectral lines between elements. Additionally, XPS is a quantitative technique. It is possible to estimate the composition of a surface without calibration to within 30% (relative) of its true value. In well-calibrated systems the relative standard deviation of measurement can be 5% or better.

TABLE 1. Analytical Characteristics of XPS[16]

Energy Range
- Kinetic Energies: 100-1500eV
- Escape Depth: 20A°
- Peak Location: + 0.1eV

Chemical Information
- Oxidation State
- Organic Structure
- Bonding Information

Elemental Sensitivity
- Elements Z > 2
- Specificity: very good
- Sensitivity Variations: 50x

Quantitative Analysis
- Absolute + 30%
- Relative + 5%
- Detection Limit: 0.1% monolayer
- Matrix Effects: some

Other Aspects
- Vacuum: 10^{-5} - 10^{-10} torr
- Depth Profiling Capability: yes slow
- x-y Resolution none
- Speed: slow typical run is 30 min
- Sample Destruction: none in 95% of the sample

EXPERIMENTAL

The catalyst samples were prepared in a continuous precipitation reactor with built-in stirrer blades as shown in Figure 3. A preheated mixed metal nitrate solution, prepared from reagent grade $Fe(NO_3)_3\ 9H_2O$ and $Mn(NO_3)_2\ 6H_2O$ diluted in deionized water, and a preheated NH_3 solution were introduced tangentially at the bottom of the reactor. The NH_3 solution was made from reagent-grade ammonium hydroxide diluted in deionized water and preheated to 85°-90°C. No attempt was made to control pH by varying feed rates since pH stayed at approximately pH 7. The precipitator was preheated and maintained at a temperature of 90°C by means of a circulating constant temperature bath. Under these conditions virtually complete precipitation occurred.[10] Table 2 shows the preparation characteristics of the catalysts.

The precipitate was collected by filtration and transferred to a vacuum oven and dried under vacuum at 140°C overnight. The dried cake was then broken up and soaked in hot water for 1-2 hours to remove occluded and adsorbed ions. The precipitate was then filtered and washed with hot water and redried under vacuum at 140°C for four hours. The catalyst was then crushed and sieved through a 325 mesh screen. A portion of the catalyst with an iron-manganese

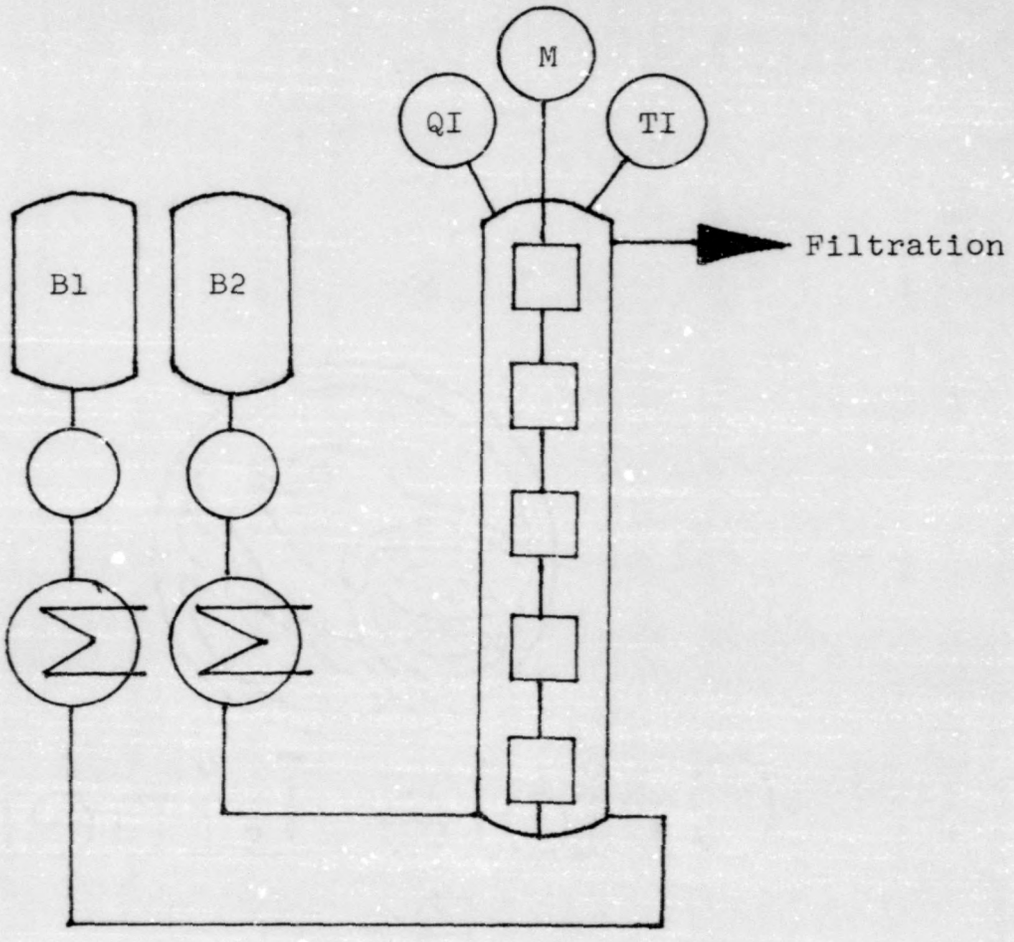

Figure 3. Apparatus for Continuous Precipitation of Catalyst

B1, B2: Vessels for solutions
QI: pH-meter
TI: Thermometer

TABLE 2. Preparation Characteristics of Iron-Manganese Catalysts

Test	Target Fe/Mn Ratio	Metals Conc. (g metal/liter)	NH_3 Conc. (%)	pH filtrate	% Fe (wt%)	% Mn (wt%)	% Fe (wt %)
SL-45	10/90	43.3	5.30	9.5	6.4	60.1	9.6
SL-43	20/80	49.6	6.72	9.2	15.0	53.8	21.8
SL-42	35/65	46.6	7.15	8.7	28.2	35.5	44.3
SL-40	50/50	46.6	7.15	9.1	36.1	27.5	56.8

ratio (wt%) of 22/78 was impregnated with K_2CO_3 to give catalysts with characteristics shown in Table 3.

The catalysts were placed in a stainless steel stirred tank reactor.[10] The feed gases (CO, H_2, He) were controlled by valves and a mass flow meter. Products and unreacted synthesis gas exited the reactor overhead via a coiled reflux condenser with a 200°C exit temperature. This stream entered a hot trap (200°C), where heavy hydrocarbons were condensed, and finally the light products were condensed from the gas stream by a series of water cooled traps. The product gas was metered by a wet test meter and could be directed to an on-line gas chromatograph that could analyze hydrocarbons up to C_8 and isomer formation up to C_4.

Unless otherwise stated, the iron-manganese catalysts in all the tests with the slurry reactor were activated in an identical manner: an in situ reduction under CO followed by synthesis condition. Fifty grams of catalyst were placed in the reactor with molten medium wax. The reactor was then sealed and purged with helium. After removal of excess slurry wax isobaric and isothermal conditions at 200 psig and 275°C within the reactor were established under He flow. At this time the He flow was stopped and CO was introduced. Activation with CO lasted for twenty-four hours at 275°C, 200 psig and a WHSV of 1.21 hr^{-1} (WHSV is defined as grams synthesis gas per hour per gram of unreduced catalyst). At the end of this activation the liquid level was readjusted

TABLE 3. Composition of Catalysts SL-62, SL-63, and SL-64

	SL-62	SL-63	SL-64
Wt% K	1.3	0.1	0.4
Wt% Mn	49.5	49.3	49.1
Wt% Fe	13.4	13.3	13.5
K/Fe ratio	.097	.008	.030

remainder of Wt% is O and C

and synthesis gas introduced. The reaction conditions were 200 psig and 275°C using a 1 H_2:1 CO feed gas.[10]

At various times during the reaction catalyst sample were extracted for XPS analysis. A mild washing of the slurry extracted samples by sonication in toluene was performed to remove the excess slurry wax. These washed samples still contained slurry wax but at a level which permitted XPS data acquisition while simultaneously preventing oxidation of the catalyst surface. The samples were either spread onto holders or pressed into thin (10 mm diameter) wafers for subsequent XPS data acquisition.

XPS data acquisition for this investigation was carried out using a Leybold Heraeus LH-10 electron spectrometer. Attached to the stainless steel ultrahigh vacuum (UHV) (Figure 4) of the spectrometer was a sample transfer [illegible] microreactor. A special feature [illegible] transfer rod which [illegible] chamber, [illegible] differentially pumped regions allowed rapid transfer from the microreactor to the analysis position of the UHV chamber.

The unused, or fresh, catalyst samples were pressed into thin wafers and placed on a molybdenum foil holder. The sample could then be transferred into the catalytic microreactors for reaction. Sample heating up to 1000°C was accomplished by direct contact between the sample and the resistively heated Mo foil boat. The temperature was

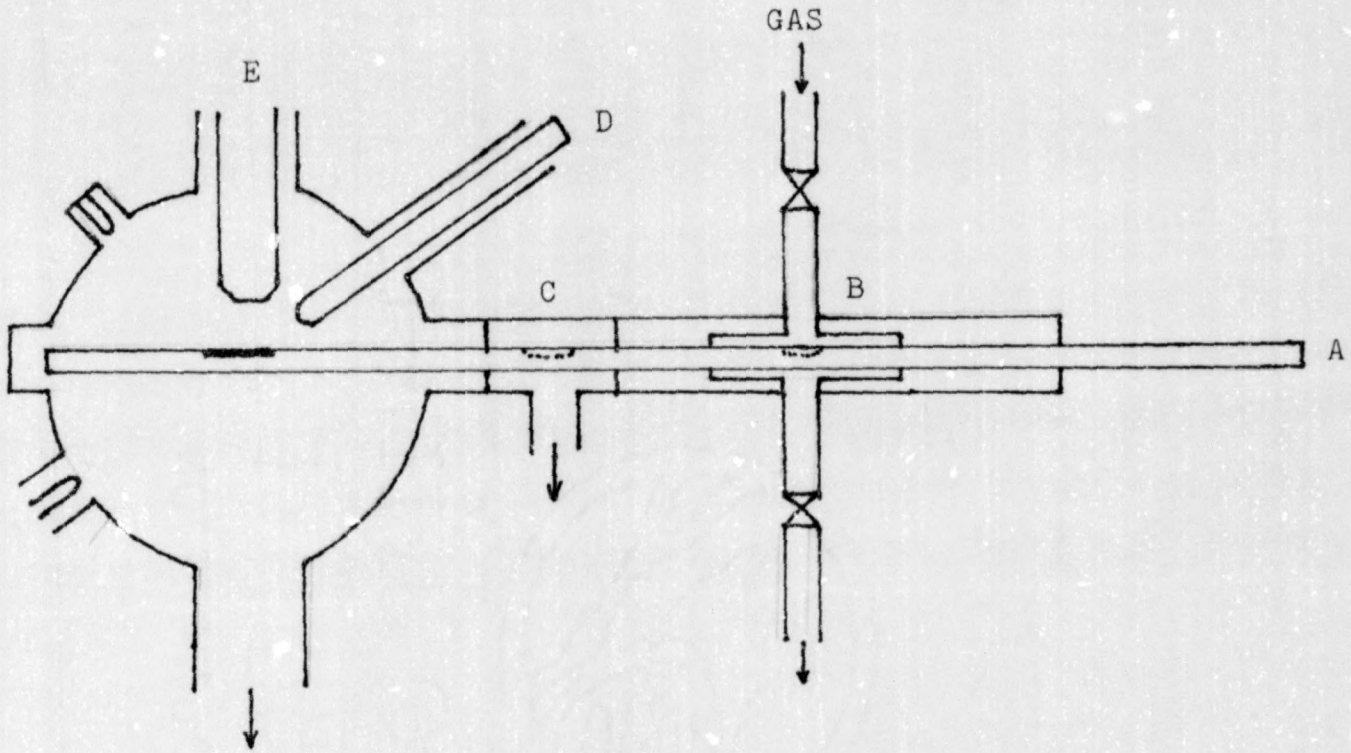

A. Transfer Rod
B. Microreactor
C. Vacuum Prep. Chamber
D. Electron Spectrometer
E. X-Ray Source

Figure 4. Diagram of XPS and Microreactor

CORRECTION

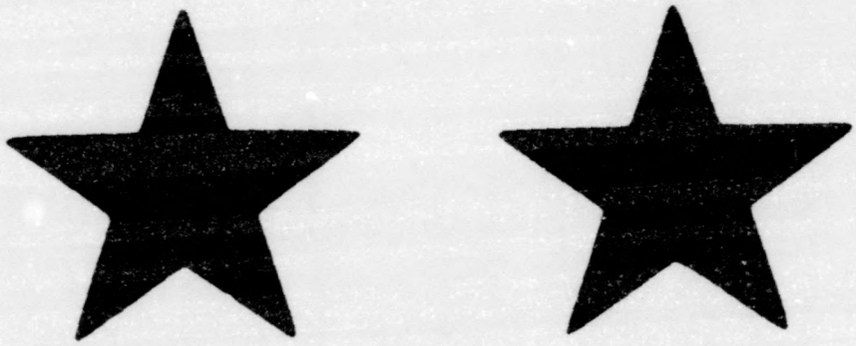

PRECEDING IMAGE HAS BEEN REFILMED TO ASSURE LEGIBILITY OR TO CORRECT A POSSIBLE ERROR

CORRECTION

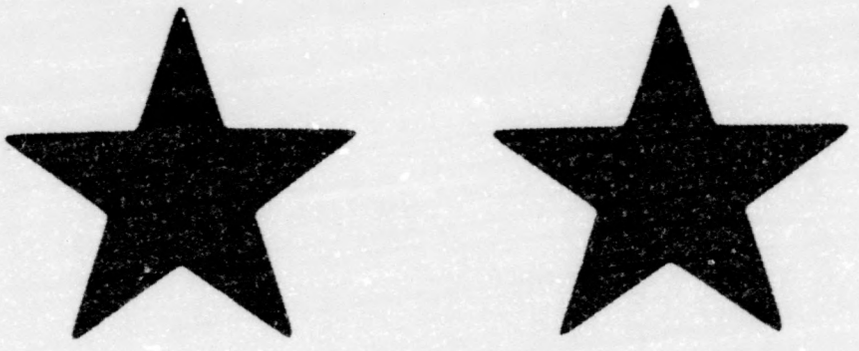

PRECEDING IMAGE HAS BEEN REFILMED TO ASSURE LEGIBILITY OR TO CORRECT A POSSIBLE ERROR

CORRECTION

PRECEDING IMAGE HAS BEEN REFILMED TO ASSURE LEGIBILITY OR TO CORRECT A POSSIBLE ERROR

and synthesis gas introduced. The reaction conditions were 200 psig and 275°C using a 1 H_2:1 CO feed gas.[10]

At various times during the reaction catalyst sample were extracted for XPS analysis. A mild washing of the slurry extracted samples by sonication in toluene was performed to remove the excess slurry wax. These washed samples still contained slurry wax but at a level which permitted XPS data acquisition while simultaneously preventing oxidation of the catalyst surface. The samples were either spread onto holders or pressed into thin (10 mm diameter) wafers for subsequent XPS data acquisition.

XPS data acquisition for this investigation was carried out using a Leybold Heraeus LH-10 electron spectrometer. Attached to the stainless steel ultrahigh vacuum (UHV) chamber (Figure 4) of the spectrometer was a sample transfer system containing a small microreactor. A special feature of this apparatus is a valve less sample transfer rod which allows the sample to be moved between UHV chamber, microreactor and atmosphere. Differentially pumped regions allowed rapid transfer from the microreactor to the analysis position of the UHV chamber.

The unused, or fresh, catalyst samples were pressed into thin wafers and placed on a molybdenum foil holder. The sample could then be transferred into the catalytic microreactors for reaction. Sample heating up to 1000°C was accomplished by direct contact between the sample and the resistively heated Mo foil boat. The temperature was

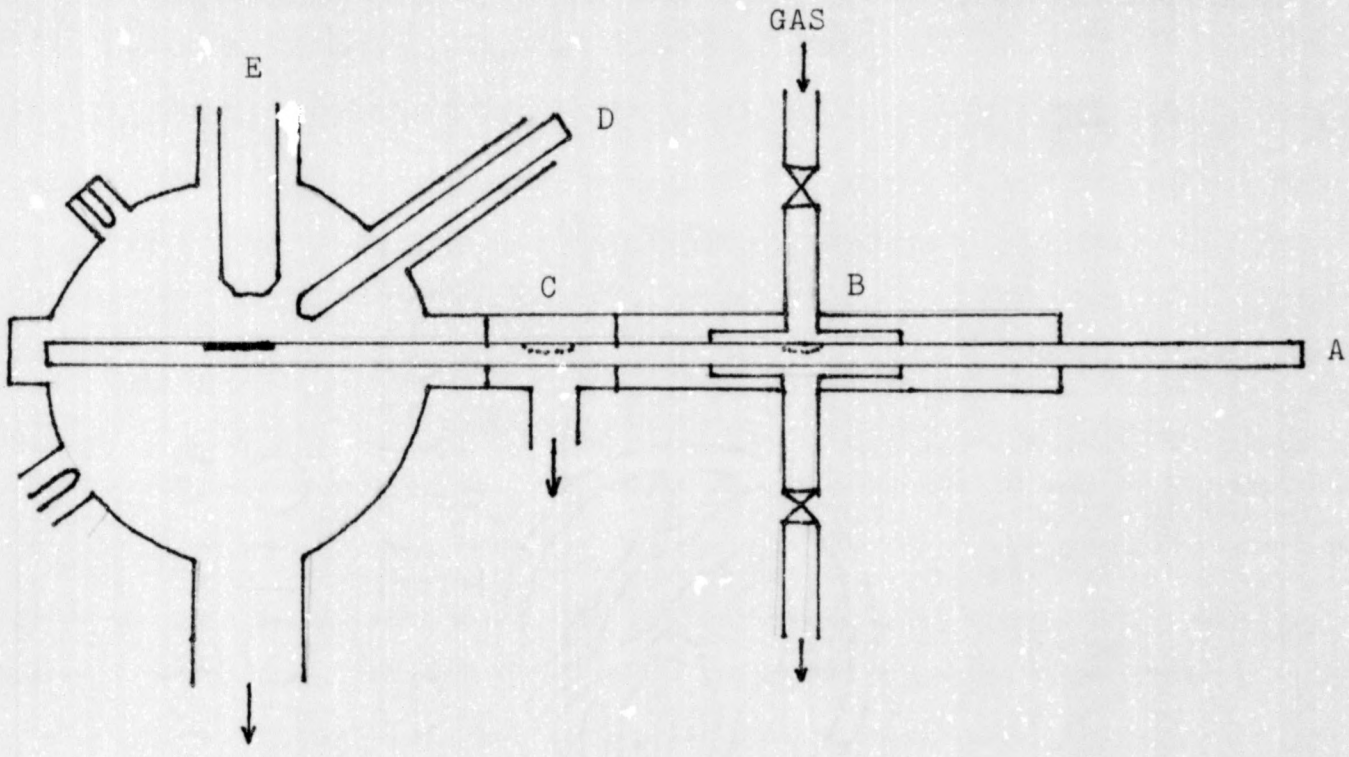

A. Transfer Rod
B. Microreactor
C. Vacuum Prep. Chamber
D. Electron Spectrometer
E. X-Ray Source

Figure 4. Diagram of XPS and Microreactor

measured by a Chromel-Alumel thermocouple attached to the underside of the foil. Various gases could be passed through the reactor, including, O_2, CO, H_2 and 1:1 synthesis gas ($CO+H_2$) at pressures up to 15 atm. For these experiments, unless otherwise stated, 15 psig pressure and a flow rate of approximately 40 cm^3/min were used.

RESULTS AND DISCUSSION

Interpretation of Spectra

A typical XPS spectrum of a fresh 20 Fe/80 Mn catalyst impregnated with 0.4% is shown in Figures 5, 6 and 7. Surface charging caused by the emission of electrons from the sample during X-ray bombardment can shift the location of XPS spectral peaks. To overcome this problem and to help with the interpretation of XPS spectral data, Table 4 includes a list of the binding energies of XPS spectral lines for known compounds. Use of this Table makes it possible to calibrate for surface charging on the catalyst samples. For example, under F-T reaction conditions, MnO cannot be reduced,[24] thus making it convenient to use the value of E_b = 641.1 eV for the Mn ($2p^{3/2}$) spectral peak when correcting for surface charging of the reduced catalyst samples.

Iron/Manganese Catalysts

Manganese is not active for the Fischer-Tropsch synthesis by itself,[26] producing only a small amount of methane. However, other investigators have noted that the specific activity of iron increases with increasing manganese to iron mass ratios for iron-manganese or coprecipitated catalysts. This promoting effect is not yet

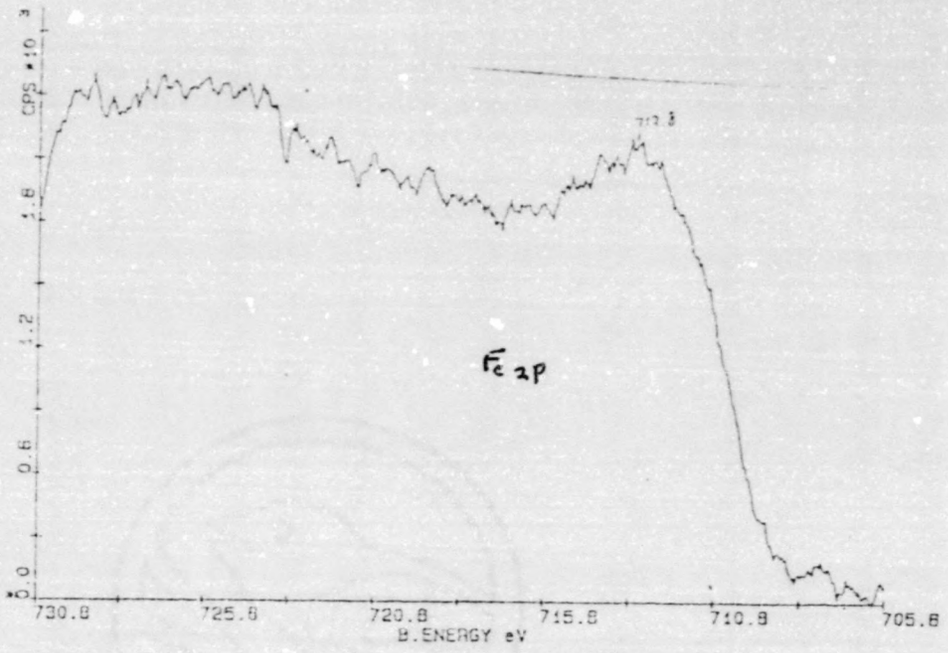

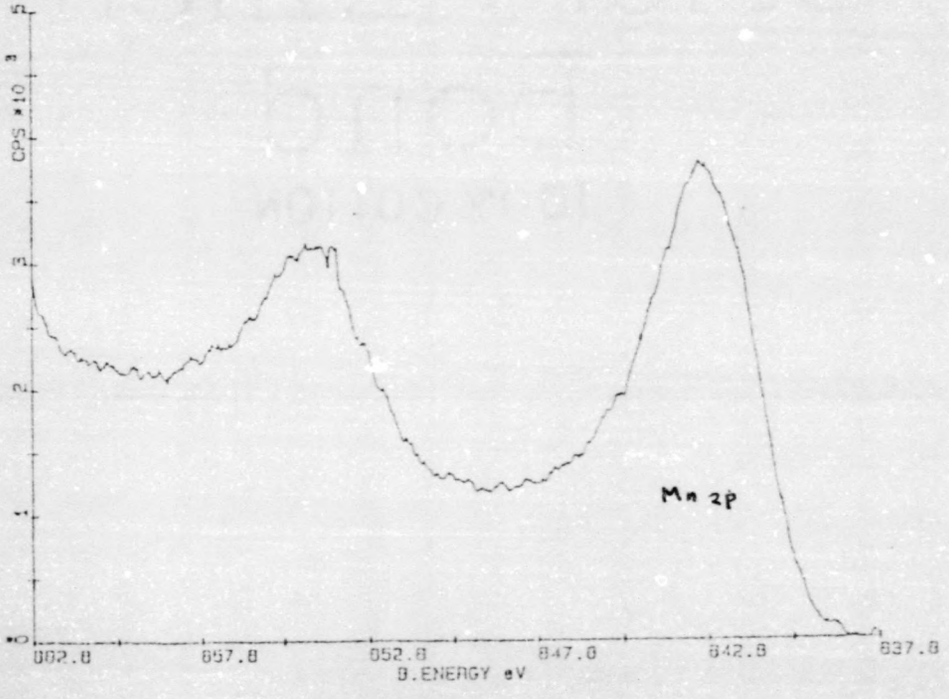

Figure 5. XPS Spectra Catalyst SL-62

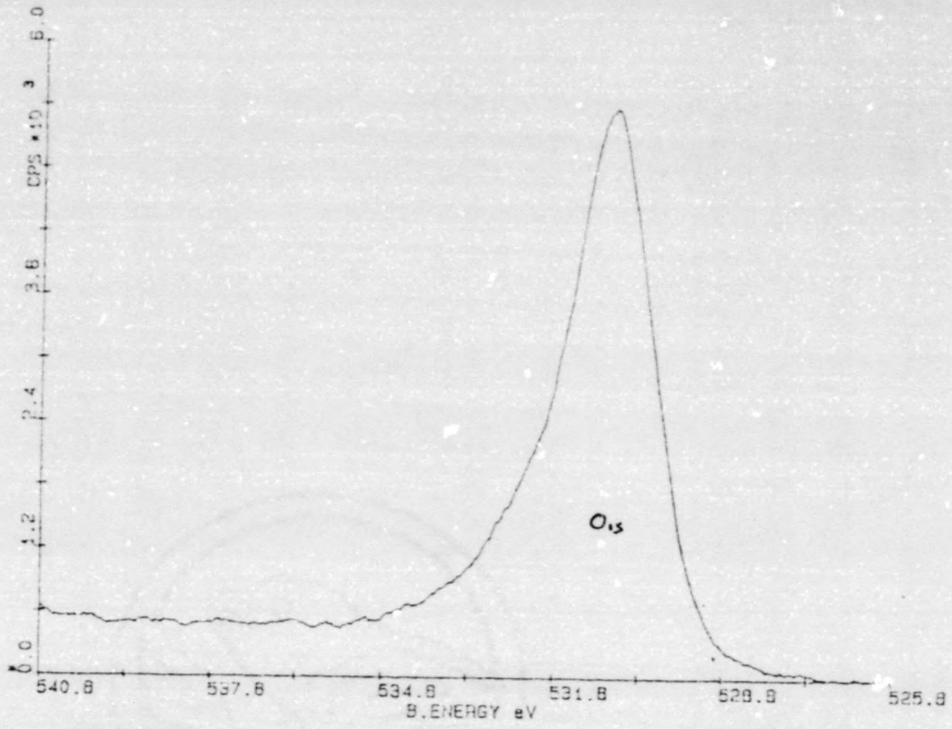

Figure 6. XPS Spectra Catalyst SL-62

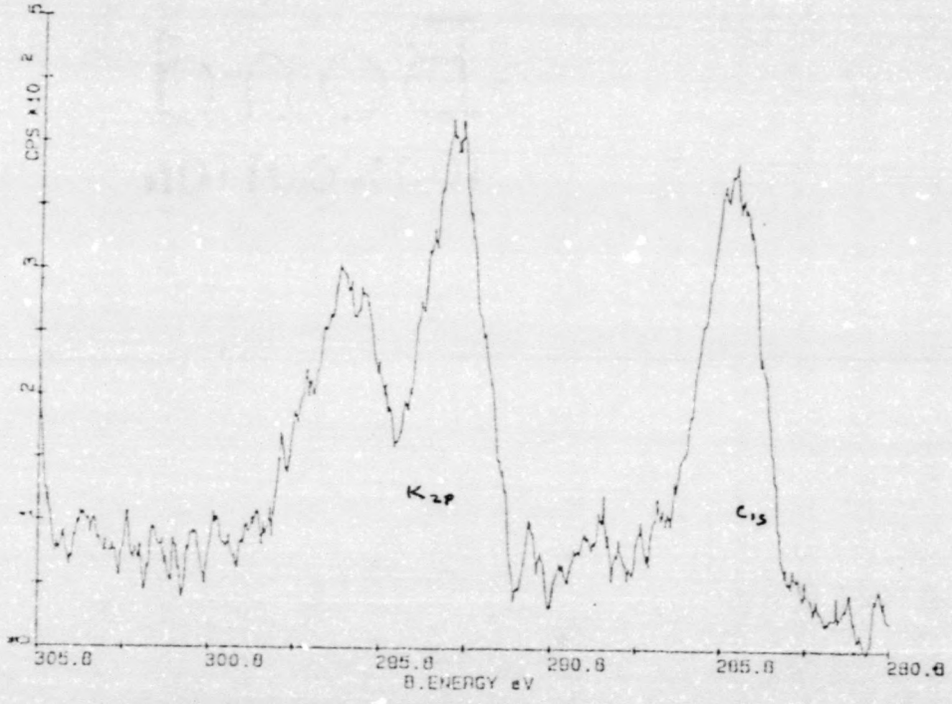

Figure 7. XPS Spectra Catalyst SL-62

Table 4. Spectral Lines of Sample Compounds

Compound	Spectral lines(eV) $Fe_{2p}3/2$	$Mn_{2p}3/2$	O_{1s}	C_{1s}	$K_{2p}3/2$	
Manganese Diron Oxide ($MnFe_2O_4$)	711.4	641.4	530.0	--	--	*
Potassium Carbonate (K_2CO_3)	--	--	532.0	290.1	293.9	(15)
High-purity graphite	--	--	--	284.6	--	(21)
Contaminated graphite	--	--	--	285.1	--	(21)
Manganese Oxide (MnO)	--	641.1	529.7	--	--	(6)
Iron metal (Fe)	707.2	--	--	--	--	(20)
Magnetite (F_3O_4)	711.8	--	530.9	--	--	(20)
FeO	710.8	--	530.3	--	--	(20)
Mn_3O_4	--	642.4	530.4	--	--	(6)

* C_{1s} at 284.6 taken as reference

fully understood and is accompanied by important selectivity changes making the Fischer-Tropsch reaction more specific.[7-10,23,26,28] Changes in the selectivity of olefin production using iron-manganese catalysts were investigated by reactor testing four catalysts with iron-manganese weight ratios of 57/43, 44/56, 22/78 and 10/90. The results of this work, performed by Pennline et al. at PETC,[10] are shown in Table 5. As can be seen from these data, the iron-manganese catalysts increase the C_2-C_4 fraction percentage and reduce the C_5^+ fraction with time on stream as compared with the fused iron catalyst which also has been reported elsewhere.[6,7,11,26] In addition, the iron/manganese catalysts tend to deactivate with time on stream.

After testing, the catalysts were recovered by filtration to remove the slurry wax and then washed in a Soxhlet extractor for 48 hours with toluene.[10] After drying under vacuum, these catalysts were analyzed by various methods. The results of analyses for fresh and used catalysts are shown in Table 6.[10] The amount of carbon added per gram of iron per hour on stream is greater for the catalysts with higher iron/manganese ratios. This increased carbon deposition can be related to a higher deactivation rate for catalysts having a high content of iron. Hence, carbon formation, or coking, could be a cause for the deactivation. X-Ray diffraction results indicate the

Table 5. Reaction Results with Iron-Manganese Catalysts

Test No. Fe/Mn Ratio	40 57/43		42 88/56			43 22/78				45 10/90			37a) Fused Iron		
Time On Stream, hrs	46	166	48	120	168	45	117	165	261	45	93	125	85	117	175
CO-Conversion, mole percent	67.1	39.2	57.9	30.7	30.0	40.3	36.1	32.6	27.0	22.2	17.9	15.5	10.1	16.9	24.8
(H_2+CO) Conversion, mole percent	61.7	30.1	58.5	31.5	30.3	38.7	34.8	31.9	25.5	23.9	19.4	17.6	9.9	16.8	19.9
Hydrocarbon Distribution, wt percent															
CH_4	8.8	11.8	9.2	13.2	12.3	6.2	6.7	7.7	8.9	7.2	8.8	10.5	9.3	8.7	8.7
C_2-C_4	30.2	38.2	35.3	37.1	35.2	31.1	35.5	38.3	39.1	35.2	35.9	39.3	36.8	20.3	21.3
C_5^+	61.0	50.0	55.5	49.7	52.5	62.7	57.8	54.0	52.0	57.6	54.3	50.2	53.9	71.0	70.0
Olefin Content C_2-C_4 Fraction, wt percent	59.5	49.6	56.7	53.7	52.8	79.5	73.7	69.1	63.8	70.7	60.0	58.9	83.7	80.9	80.8
Internal/Terminal-Olefin Ratio of Oil Product	0.61	---	.56	2.38	---	.26	.61	1.15	---	.86	---	1.75	.09	.08	.07
cis 2-Butene/1-Butene Ratio	0.26	0.37	.21	.31	.33	.08	.15	.19	.27	.18	.27	.44	0	0	.05
Liquid Oil Product Composition, vol. percent															
Aromatics	8	5	8	7	8	11	11	11	9	7	7	6	10	8	9
Olefins	68	60	65	58	67	72	67	66	62	73	63	53	77	84	78
Saturates	27	35	27	39	24	37	22	23	28	20	30	41	13	10	13
Chain Growth Probability	0.69	.68	.66	.60	.62	.67	.66	.63	.56	.66	.64	.61	.69	.72	.75
C_1-Experimental/ C_1-Theoretical	0.99	.96	.82	.98	.91	.71	.65	.53	.52	.75	.76	.61	1.07	1.12	1.09

a) 1.71 WHSV, 250°C, 200 psig.

Table 6. Fresh and Used Catalyst Analyses

Test	SL-40		SL-42		SL-43		SL-45		SL-47	
Fe/Mn Ratio	57/43		44/56		22/78		10/90		Fused-Iron	
	Fresh	Used	Fresh	Used	Fresh	Used	Fresh	Used	Fresh	Used
Time on Stream, hours	---	166	---	237	---	309	---	223	---	418
Chemical Analysis, at percent										
C	<.3	11.6	---	13.4	<.3	7.4	<.3	2.9	<.3	7.6
H	1.0	0.6	---	0.8	0.6	0.6	0.3	<.3	<.3	0.5
S	<.07	<.07	---	<.07	<.07	<.07	<.07	<.07	<.07	<.07
K	<.095	<.095	---	<.095	<.095	<.095	<.095	<.095	0.4	0.3
Fe	35.0	31.4	28.2	21.4	12.0	14.5	6.8	7.4	66.3	70.2
Mn	24.8	21.8	35.5	27.9	51.4	52.3	58.6	59.5	<.095	0.4
BET Surface Area, m^2/gm	150.0	29.2	121.5	22.6	76.5	31.7	59.9	25.5	1.3	4.6
Mean Pore Diameter, Å	43	216	72	183	93	183	100	229	---	309
X-Ray Diffraction										
Fresh	Mn_3O_4[Z]		Mn_3O_4[Z]		Mn_3O_4[Z]		Mn_3O_4[Z]		Fe_3O_4	
Used		Fe_3O_4, $MnCO_3$ + unidentified minor phase		Fe_3O_4, $MnCO_3$ + Minor FeC		MnO*		MnO*		Fe_3O_4 + Minor Fe_2C

Note: Z = Fe may be present in solid solution with Mn_3O_4 or γ-Mn_2O_3.
* = Fe may be present in solid solution with MnO.

existence of an iron carbide phase for the samples SL-40 and SL-43 which have the highest and second highest iron/manganese ratio of the four iron-manganese catalysts studied. Although iron carbide was not detected in the catalysts having smaller iron concentrations, lack of such detection may be due to limitations in the X-ray analysis. A manganese carbonate phase is observed in the two catalysts with the highest iron concentrations.

Fresh samples of the same catalysts used in the slurry reactor experiments were pressed into wafers and inserted into the XPS-microreactor system. Each sample was first analyzed in its original condition then transferred to the microreactor and exposed to CO gas at 15 psig for 1 hour at 300°C. The sample was then transferred back to the UHV chamber for XPS analysis. The sample was then returned to the microreactor and exposed to 1:1 CO/H_2 gas mixture at 15 psig for 1 hour at 300°C. The sample was again transferred to the UHV chamber for XPS analysis. After data acquisition the sample was returned to the microreactor and exposed to H_2 gas at 15 psig for 1 hour at 300°C. The sample was then reanalyzed.

Each sample, except SL-43, was subjected to this sequence of exposures to give an indication of the processes of activation, reaction, and removal of hydrocarbon products form the surface of the catalyst sample. SL-43 was exposed an additional 17 hours to the 1:1 CO/H_2 gas mixture at 15

psig and 300°C to see if significant changes occurred in the catalyst surface. Table 7 shows the iron/manganese and carbon/manganese ratios after each microreactor exposure.

The data in Table 7 show that the carbon/manganese ratios decrease with decreasing iron concentration in the fresh catalyst samples in the order of SL-40 > SL-42 > SL-43 > SL-45. This trend is repeated after exposure to CO, synthesis gas, or H_2. The carbon/manganese ratio also increases with exposure to CO. These trends are consistent with the data obtained with the slurry reactor. The major trend noted was a decrease in iron/manganese ratio with increasing exposure time to CO or synthesis gas. The implications of this decrease coupled with the inability to detect any iron carbide or metallic iron will be discussed below. The spectral line positions obtained from XPS analysis of the samples are shown in Table 8.

The positions of the $Mn_{2p}3/2$ peak for the exposed catalysts sampled are typical for that of MnO (E_b= 641.1 eV).[6] The O_{1s} peak is also similar to that for MnO (O_{1s}, E_b= 529.7[6]) Therefore, manganese is possibly present as MnO on the catalysts after activation with CO or reaction with CO/H_2 mixtures. This observation is reasonable since below 1200°C MnO cannot be reduced.[30]

The trend of the C_{1s} binding energies with increasing iron concentration in the catalysts supports the X-ray diffraction data which show that iron carbide is present in

TABLE 7. Atomic Ratios, Fe/Mn and C/Mn, from XPS Analysis

	SL-40	SL-42	SL-43	SL-45
Fe/Mn ratio				
bulk	57/43	44/56	22/78	10/90
Fresh	.831	.387	.269	.265
CO, 1 hour at 300°C	.621	.302	.198	.207
CO/H_2, 1 hour at 300°C	.456	.402	.172	.195
H_2, 1 hour at 300°C	.643	.331	--	.215
CO/H_2, 18 hours at 300°C			.163	
C/Mn ratio				
Fresh	2.54	2.36	1.60	1.40
CO, 1 hour at 300°C	4.32	2.13	1.74	.95
CO/H_2, 1 hour at 300°C	6.20	2.71	1.82	1.21
H_2, 1 hour at 300°C	5.23	2.72	--	1.51
CO/H_2, 18 hours at 300°C			2.40	

TABLE 8. XPS Spectral Line Positions for Reduced Fe/Mn Catalyst Samples

	Spectral Lines (eV)			
	Fe	Mn	O	C
SL-45 10 Fe/90 Mn				
Fresh	714.1	644.0	532.1	266.3
CO/300°C/1 hr	713.0	641.1	530.1	284.9
$CO+H_2$/300°C/1 hr	713.0	641.1	530.0	284.6
H_2/300°C/1 hr	712.5	641.0	530.0	284.6
SL-43 20 Fe/80 Mn				
Fresh	714.1	643.6	531.4	285.6
CO/300°C/1 hr	713.1	641.2	530.2	285.2
$CO+H_2$/300°C/1 hr	713.1	641.2	530.3	285.0
$CO+H_2$/300°C/16 hr	713.1	641.4	530.2	285.1
SL-42 35 Fe/65 Mn				
Fresh	713.5	643.6	531.6	285.8
CO/300°C/1 hr	712.1	641.1	530.0	284.6
$CO+H_2$/300°C/1 hr	712.2	641.0	530.1	284.5
H_2/300°C/1 hr	712.4	641.1	530.0	284.5
SL-40 50 Fe/50 Mn				
Fresh	713.1	643.7	531.7	286.0
CO/300°C/1 hr	711.5	641.0	530.1	284.5
$CO+H_2$/300°C/1 hr	711.6	641.1	530.2	284.2
H_2/300°C/1 hr	711.5	641.1	530.2	284.2

samples of high iron content. This shift toward lower binding energies represents a shift toward values in agreement with those for iron carbide (283.3 eV).[20] The iron $2p^{3/2}$ peak also shifts toward lower binding energies with increasing iron content in the catalysts.

Surface structural properties are expected to influence the catalytic activity and selectivity of iron/manganese during F-T synthesis reactions. Only recently have such structural properties and their effects been investigated for iron-manganese catalysts.[12,24,27,28] From the previous data presented, it is apparent that substantial changes occur in the catalyst surface during CO or H_2 reduction. From the X-ray diffraction data the major manganese component is Mn_3O_4. A solid solution can form between Mn_3O_4 and Fe_3O_4. The presence of a solid solution after activation is in agreement with the observations of other workers.[24,27] However, such a solution cannot be identified within the present work. The positions of the $Fe_{2p}3/2$ and $Mn^{3/2}$ (Table 9) for the fresh sample with respect to the C_{1s} binding energy of 285 eV indicate the possibility of a strong electronic inaction between manganese and iron since substantially higher binding energies are found than would be expected for Fe_3O_4 ($Fe_{2p}3/2$ = 711.8) or Mn_3O_4 ($Mn_{2p}3/2$ = 641.8).

The data presented in Table 8 show that for all catalyst samples after reduction in CO the binding energy of the

TABLE 9. XPS Spectral Line Positions for Fresh Fe/Mn Catalysts

	Spectral Lines		
Catalysts	$Fe_{2p}3/2$	$Mn_{2p}3/2$	O_{1s}
SL-45	713.4	642.7	530.8
SL-42	713.5	642.8	530.8
SL-42	712.5	642.8	530.8
SL-40	712.1	642.7	530.8

$Mn_{2p}3/2$ peak assumes a value indicative of MnO ($Mn_{2p}3/2$ = 641.1 eV). This change is consistent with the X-ray diffraction data in Table 6 and is also consistent with the fact that under F-T synthesis conditions MnO cannot be reduced. The $Fe_{2p}3/2$ peak positiion is also shifted toward lower binding energies (after CO exposure). In the case of the SL-40, the value for the $Fe_{2p}3/2$ approaches that for FeO ($Fe_{2p}3/2$ = 710.8 eV). Such a binding energy indicates the formation of a solid solution of MnO with FeO.[10] Another possibility is the formation of the $MnFe_2O_4$ spinnel during reduction. X-ray diffraction studies of reduced iron-manganese catalysts have suggested the presence of this spinel.[24] Its presence is also consistent with the XPS data for the $Fe_{2p}3/2$ ($MnFe_2O_4$, $Fe_{2p}3/2$ = 711.4 eV) and $Mn_{2p}3/2$ ($MnFe_2O_4$, $Mn_{2p}3/2$ = 641.4 eV) peaks for catalyst sample SL-40. However, the formation of a solid solution of FeO-Mn or the formation of a spinel would make reduction beyond Fe^{2+} or Mn^{2+} thermodynamically difficult.[29]

As reported above, no metallic iron or iron carbide was observed during XPS analysis of the reduced samples. Additionally, the iron/manganese ratios decreased during reduction. This result is surprising since metallic iron and iron carbide are considered to be the active phases of the catalyst during F-T synthesis.[22] In more recent experiments at PETC[29] the surfaces of reduced iron-manganese catalysts were sputtered with argon ions to remove several A^{o} of the surface of the catalysts. This sputter

removal then allowed the detection of metallic iron and iron carbide. Similar findings have been reported for iron-manganese alloys[25] that were reduced with CO gas. In this latter case, it was found that while the iron oxides were reduced to metallic iron, the reduction of the manganese oxide was only to MnO. In addition, the concentration of MnO increased with reduction time. This phenomenon is commonly observed in steels containing manganese.[25] Similar results have been reported for iron-manganese catalysts in H_2 at 500°.[27]

Table 8 also shows that the binding energy of the $Fe_{2p}3/2$ peak decreases with increasing iron content. This change may suggest that the primary effect of manganese is electronic, if it is assumed that a higher concentration of manganese increases such an electronic effect.

Potassium Promoted Iron-Manganese Catalysts

The promoting action of potassium and its chemical nature in working catalysts have been the subject of intense research.[13-15,21,22] Although potassium can be initially added as KOH, KNO_3, or K_2CO_3, the promoting effect during the synthesis reaction seems to be independent of its initial state.[15] Frequently, the active form of the promoter is referred to as K_2O[14]; recently, the form KOH has also been suggested.[15]

To investigate the behavior of potassium promoted iron/manganese Fischer-Tropsch catalysts, a 20 Fe/80 Mn catalyst was impregnated with varying amounts of K_2CO_3

(Table 3). Each of the resulting promoted iron-manganese catalysts was reacted in a stirred slurry reactor with identical activation procedures and initial process conditions of 275°C, 200 psig and 1.2 WHSV of 1 H_2/1 CO synthesis gas. Samples were withdrawn at various times during the operation of the reactor for XPS investigation.

The results of these slurry reactor runs performed by Hank Pennline at PETC are shown in Table 10. These data show that only at high potassium loadings do the iron-manganese catalysts behave similarly to promoted iron catalysts. In particular, it can be seen that with 1.3% potassium

1) the CO conversion increases

2) methane product decreases

3) weight percent fraction of C_5^+ increases

In addition, the olefin content increases with increasing potassium. The CO conversion in the product activity is as follows:

$$SL\text{-}60 \sim SL\text{-}63 < SL\text{-}64 < SL\text{-}62.$$

Similar trends have been reported by other researchers for supported iron catalysts[22] in which the activity of the catalyst changed markedly when potassium concentrations were greater than 1.0%.

The XPS analyses of the promoted iron-manganese catalyst samples withdrawn during operation of the slurry reactor were used to determine the surface concentrations of iron, manganese, and carbon. The results are given in

Table 10. Reaction Results with Promoted Iron-Manganese Catalysts

Test	SL-60				SL-63		SL-64			SL-62		
Time on Stream, hrs	48	120	204	272	48	119	46	118	187	47	119	191
CO-Conversion, mol percent	35.7	32.4	29.1	27.1	32.9	14.6	56.3	32.9	18.0	59.5	40.5	30.4
Hydrocarbon Distribution, wt%												
CH4	6.9	7.2	7.8	8.3	7.0	16.6	9.4	9.5	6.6	4.9	3.6	3.8
C2-C4	38.3	39.1	40.7	42.4	32.3	48.8	37.6	37.1	29.3	27.5	23.4	25.1
C5	54.8	53.7	51.5	49.3	60.7	34.6	53.0	53.4	64.1	67.6	73.0	71.1
Olefin content C2-C4 Fraction, wt%	76.8	72.3	68.8	67.2	65.4	45.4	65.2	67.4	69.3	83.8	84.4	85.9

Table 11. In general, the iron/manganese ratios increase for equal times on stream in the order of slurry runs (SL-60)<(SL-63)~(SL-62)<(SL-64). No trend is seen in the iron/manganese ratios as a function of time on stream for each slurry run. The carbon/manganese ratios increase with increasing time on stream for each slurry run. In general, for the Soxhlet extracted samples the promoted samples tend to have higher carbon/manganese ratio than the unpromoted catalysts. Also, there is a trend in increasing carbon/manganese ratios and decreasing CO-conversion (Table 10) with increasing time on stream for each slurry run.

The increase in the carbon/manganese ratios in Table 11 is related to carbon deposition as a function of time on stream and/or a difference in the amount of slurry wax retained by the catalysts after toluene sonication. Increased amounts of carbon on potassium-promoted catalysts as compared to unpromoted catalysts after use agree with the observation by other researchers that potassium promotes the rate of carbon deposition.[13] It is also in general agreement with the observations of other workers[14] that deactivation of the catalysts can be related to the deposition of surface carbon.

No iron carbide or completely reduced iron was observed during XPS examination of the used catalysts. This observation is considered surprising since the reaction

TABLE 11. Atomic ratios, Fe/Mn and C/Mn from XPS Analysis of Promoted Iron-Manganese Catalysts.

	SL-60	SL-63	SL-64	SL-62
Fe/Mn after	(0% K)	(0.1% K)	(0.4% K)	(1.3% K)
CO Activation	0.16	0.18	0.29	
~ 45 hr	0.16	0.20	0.53	0.16
~145 hr		0.28		
~200 hr	0.15		0.50	0.24
~350 hr	0.17		0.45	0.34
Soxhlet	0.27	0.20	0.42	0.18
C/Mn after				
CO Activation	10	7	8	
~ 45 hr	19	13	23	16
~145 hr		15		
~200 hr	52		59	34
~350 hr	50		60	65
Soxhlet Ext.	12	15	25	17

conditions should have completely reduced or carburized these catalysts.

The catalyst SL-62 was placed in the XPS microreactor and reduced under H_2 at 300°C for 1 hr, 2 hr, and 3 hr. The XPS spectra for the K_{2p} and C_{1s} peaks are shown in Figure 8. The most notable aspect of these is the increase in the intensity of the $K_{2p}3/2$ peak at approximately 295.6 eV (E_b = 293.4 eV corrected to Mn ($2p^{3/2}$) = 641.1 eV) with increasing reduction time. Additionally, the carbonate $C^{(15)}$ peak at E_b = 292.0 eV also increases in intensity.

Each of the three potassium impregnated catalysts were reduced for various times (1/2 hour, 1 hour, 2 hours, 16 hours) using either CO or H_2 as the reducing gas. For each catalyst the amount of surface potassium increases to some maximum potassium/manganese value. Table 12 indicates that this maximum is dependent on the initial K_2CO_3 loading. This maximum was reached within 1 or 2 hrs. of initiation of reduction. Other investigators[22,14] have speculated that potassium must be in contact with the iron to be an effective promoter. Hence, the increase in selectivity of the promoted catalyst (SL-60 ~ SL-63 < SL-64 < SL-62) with increasing K_2CO_3 loading may be explained in terms of increasing potassium coverage of the iron surface. With the iron/manganese catalyst, potassium can deposit either on the Mn(0) on the iron surface. The partitioning of potassium between the Mn(0) and iron is unknown. However, with more

Figure 8. XPS Spectra of K_{2p} and C_{1s} Spectral Peaks After H_2 Exposure

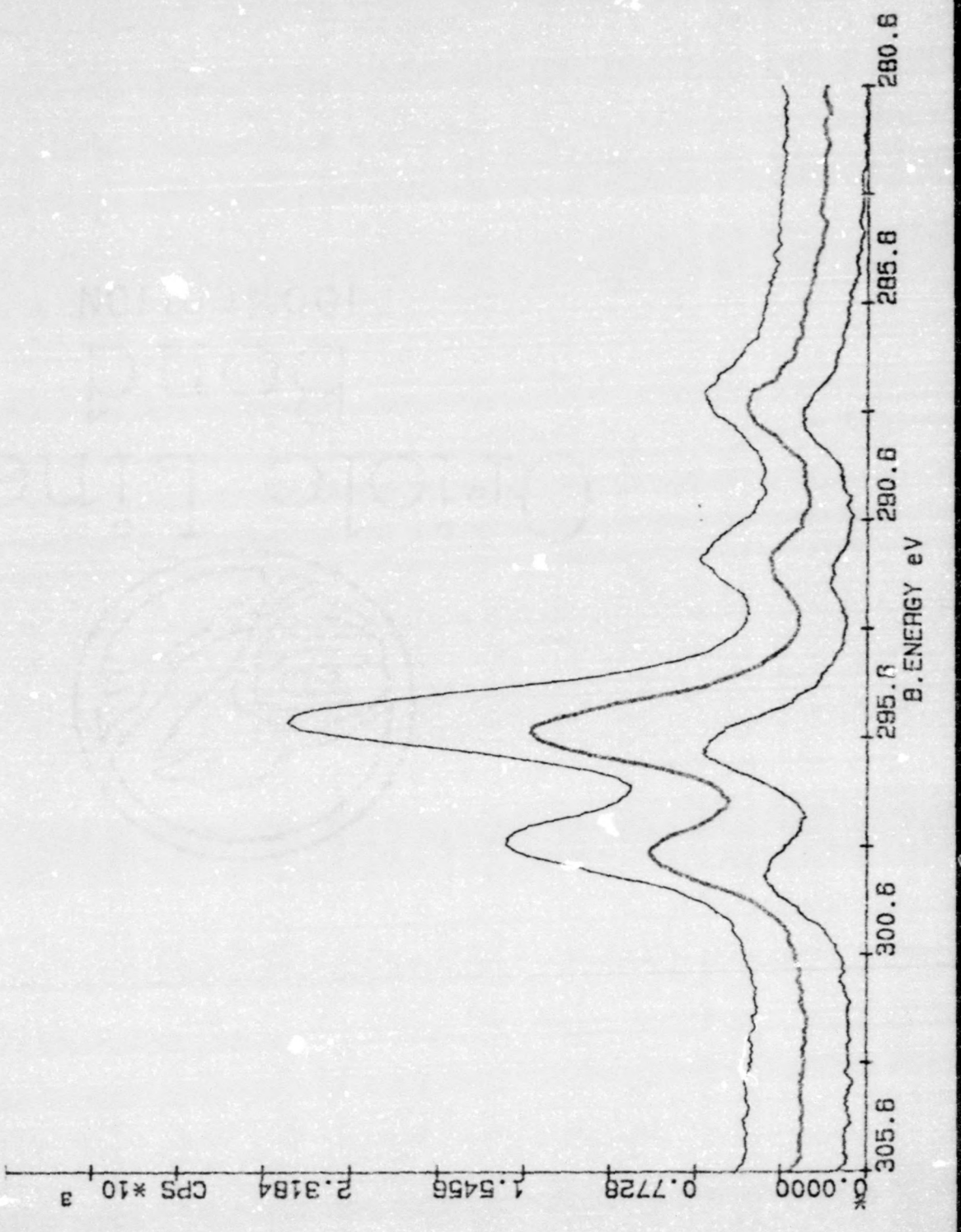

Table 12. Comparison of K/Mn ratio

	Max K/Mn ratio obvs.
SL-63 (0.1%K)	.149
SL-64 (0.4%K)	7.68
SL-62 (1.3%K)	30.2

potassium the surface iron is more thoroughly covered by alkali thereby causing an altered product selectivity.

The observation that the amount of carbonate (CO_3) on the catalyst surface increases with increasing potassium content suggests that the major potassium species on the activated catalyst surface is K_2CO_3. To investigate this possibility, the data for the reduction of SL-62 in H_2 was scrutinized.

In addition, the O_{1s} peak for SL-62 was also investigated (Figure 9). These data show that, in addition to the already described intensity increases in potassium $K(2p^{3/2})$ peak and the carbonate C_{1s} peak with reduction time, there is a significant change in the O_{1s} peak. The shoulder at E_b = 533.6 eV increases in intensity with increasing reduction time while the main O_{1s} peak at E_b = 532.4 eV decreases in intensity. Since this shoulder is at a position which is indicative of carbonate oxygen it supports the supposition that the potassium is present as K_2CO_3.

To further confirm that K_2CO_3 was the major surface species of potassium, the stoichiometry of potassium, carbon, and oxygen was determined to see if it was consistent with K_2CO_3. First, the area under peak of interest was determined for each reduction time. The area for the O_{1s} spectra was obtained by deconvolution of its two overlapping peaks. In this way the area of the carbonate O_{1s} shoulder could easily be determined. Next, the change in area of each peak of interest as a function of reduction

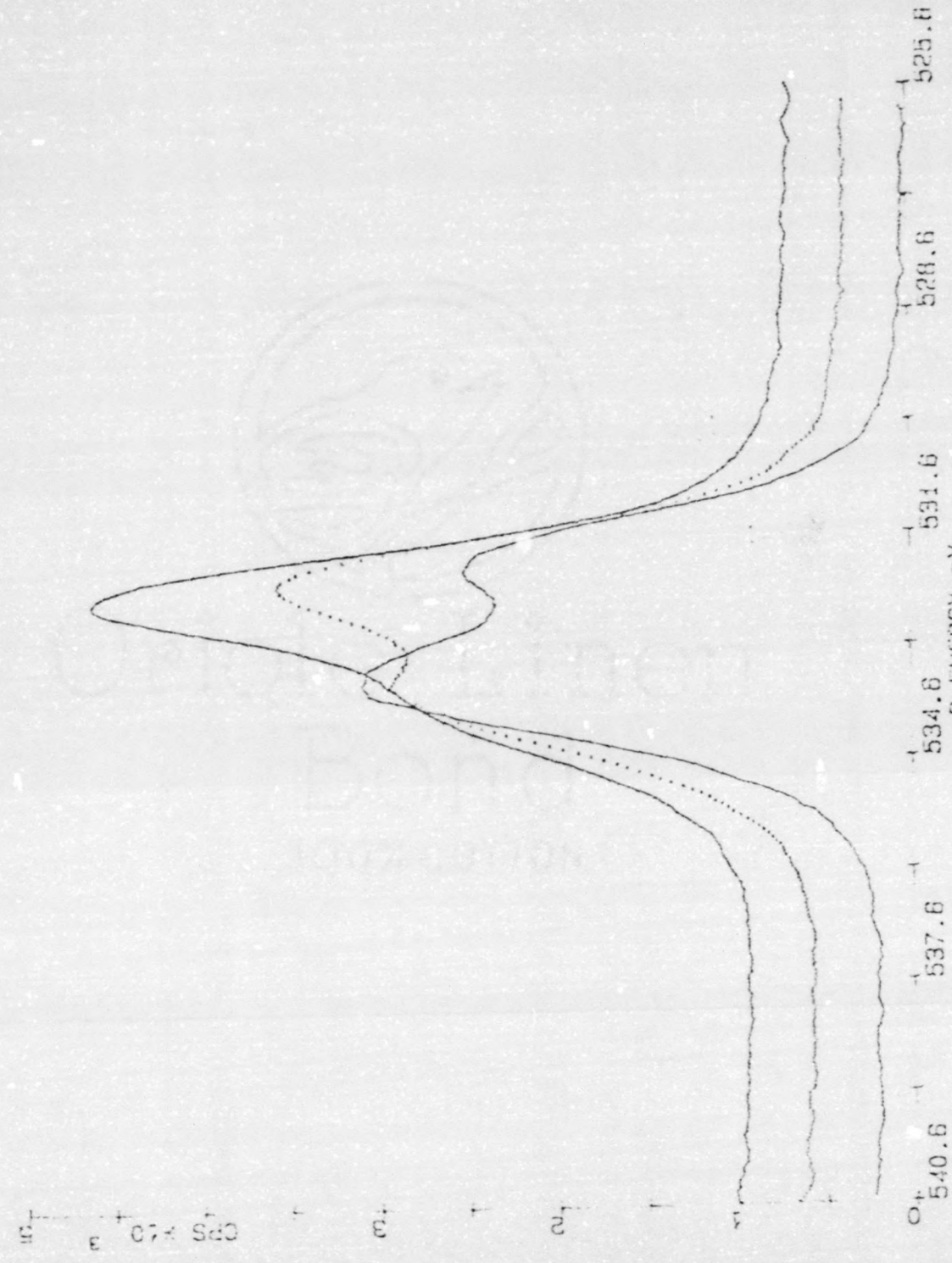

Figure 9. XPS Spectra of O_{1s} Spectral Peak After H_2 Exposure

time was determined by subtracting peak areas as shown in Figure 10. This change in peak area is related to the change in surface concentration of each element during reduction. To find the relationship between the elements, potassium, carbon (carbonate), and oxygen (carbonate), the change in area of the $K(2p^{3/2})$ and the O_{1s} (carbonate) peaks were divided by the change in area of C_{1s}(carbonate) peak. The peak areas were corrected for differences in sensitivity of XPS detection. These data, summarized in Table 13, show that the stoichiometry of the elements potassium, carbon, and oxygen is very close to that for K_2CO_3.

Other experiments with CO as the reducing agent or with other catalyst of different potassium loading (SL-63 or SL-64) gave similar results. However, it is worth noting that the value for potassium varied between 1.1 to 1.8. The 1.1 value is significantly lower than the expected value of 2. The potassium promoted catalysts (SL-64, SL-63 and SL-62) were also reduced at higher temperatures of 450° to 500°C for one hour under H_2 to determine the effect of high temperature treatment on the potassium species. These data showed that a substantial amount of carbonate was still present.

The samples must be transferred from reaction conditions to a high vacuum region for XPS analysis. During this transfer there is a possibility of change in the surface composition of the sample despite precautions.

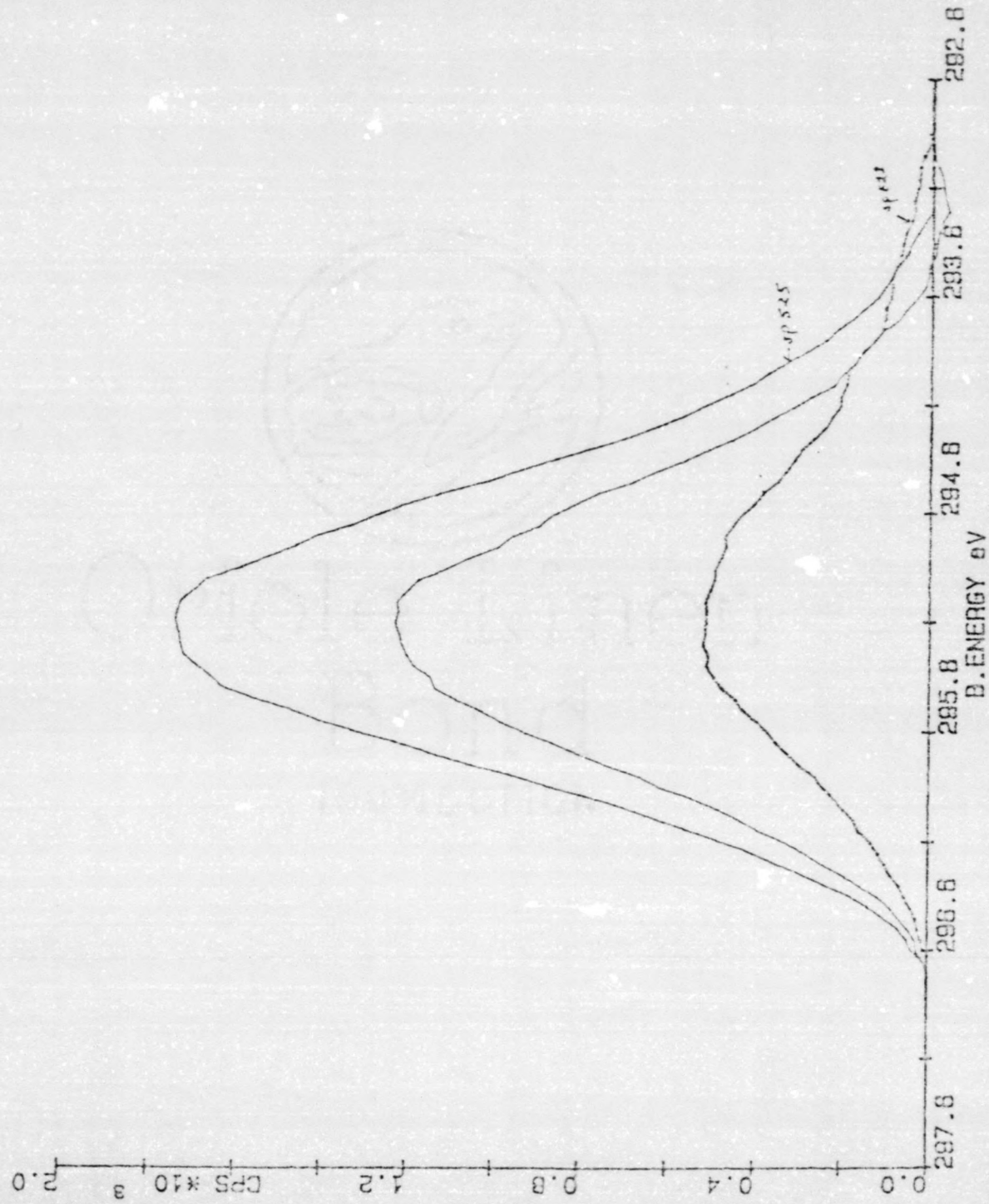

Figure 10. Subtraction of Spectral Peak Areas

Table 13. Spectral Peak Area Changes During Reduction

	Change in Area		
	O	K	C
sp 525-523 H_2/300 C/1hr	1623	1856	214
sp 525-524 H_2/300 C/2hr	960	1055	103
sp 524-523 H_2/300 C/3hr	900	827	113

K/C =

	K/C	O/C
sp 525-523	1.6	2.5
sp 525-524	1.9	3.0
sp 524-523	1.3	2.6

formula $K_{1.3-1.9}CO_{2.5-3.0}$

However, a strong carbonate peak in these potassium-containing samples was noted even after 16 hours of reduction in H_2 at 300°C. If significant amounts of KOH or K_2O were present the potassium/carbon value would be significantly higher than 2 since each potassium ion associated with an OH^- or $O^=$ ion would raise the potassium formula value in relationship to carbon. Definitely, the results reported herein are different from those reported by others for iron foils which indicate KOH as the major active species.[13-15] This difference may be related to the presence of $MnCO_3$ on the surface. Investigators at PETC have observed $MnCO_3$ to be present in similar unpromoted and used iron-manganese catalysts.[10] Thus, the presence of $MnCO_3$ may account for the lower potassium formula value and effect the chemical nature of potassium on the surface of the iron-manganese catalyst by providing a reservoir of surface CO_3.

CONCLUSIONS

The XPS investigation of the precipitated iron-manganese catalysts and potassium promoted iron-manganese catalysts produced several results which can be summarized as follows:

1. Potassium promotes iron-manganese catalysis in a similar fashion as iron catalysis by
   a) Increasing velocities of CO consuming reactions
   b) Suppressing the formation of methane
   c) Increasing chain growth
   d) Increasing the olefin content of reaction products.
2. However, the loading of potassium with respect to iron to affect these changes is much larger in iron-manganese catalysts than in iron catalysts. Potassium coverage of surface increases during reduction. A maximum potassium coverage occurs that depends on the reduction time and the initial potassium loading.
3. The predominate speciation of potassium on the surface of the catalyst was K_2CO_3 after H_2.
4. During reduction of the catalyst the surface iron/manganese ratio decreases due to the migration of MnO over the iron.
5. The binding energy for the $Fe_{2p}3/2$ peak shifts to values with decreasing manganese concentration.

REFERENCES

1. J. Haggin, Chem. and Eng. News, 59, 39 (81).

2. B. Bussemeier, C. D. Frohning, and B. Cornils, Hydrocarbon Processing,11, 105 (1976).

3. C. K. Rofer-De Poorter, Chem. Rev., 81, 447 (1981).

4. R. C. Brady and R. Pettit, J. Am. Chem. Soc., 103(5), 1287 (1981).

5. H. Scherlz and A. Zein el Deen, Fuel Processing Technology, 1, 45 (1977).

6. J. Barrault, and C. Renard, Nouveau J. Chim., 7(3), 149 (1983).

7. H. Kolbel, M. Rolek, and K. D. Tillmetz, Proc. 13th Intersoc. Energy Conv. Eng. Conf., Society of Automot. Engrs.; paper No. 789,494 (1978).

8. H. Kolbel, and K. D. Tillmetz, U.S. Patent 4,177,203, 1979.

9. H. Schulz and H. Jokcebay, Proc. Organic React. Soc. Conf., Charleston, SC, April 1982.

10. H. W. Pennline, M. F. Zarochak, R. E. Tischer, and R. R. Schell, DOE Report, U.S. Department of Energy, 1984.

11. H. J. Lehman, M. Ralek, and W. D. Deckwer, Paper No. 103d presented at 73rd Annual Meeting AIChE, Chicago, November 1980.

12. W. L. Van Dijk, J. W. Numantsverdriet, A. M. Van Der Kraan, and H. S. Van Der Bean, Appl. Catal. 2,273 (1982).

13. H. P. Bonzel and H. J. Krebs, Surface Science, 109, 2527 (1981).

14. J. Benziger and R. J. Madix, Surface Science, 94, 119 (1980).

15. H. P. Bonzel, G. Broden, and H. J. Krebs, Applications of Surface Science 16, 373 (1983).

16. D. M. Hercules and S. H. Hercules, J. Chem. Ed., 61(6), 483 (1984).

17. I. Adler, L. I. Yin, T. Tsand, and G. Coyle, J. Chem. Ed., 61(9), 757 (1984).

18. Deckwer, Y. Serpemen, M. Rolek, and B. Schmidt, Ind. Eng. Chem. Process Des. Dev., 21, 222 (1982).

19. H. J. Krebs, H. P. Bonzel, and W. Schwarting, J. Catalysis, 72, 199 (1981).

20. D. J. Dwyer and J. H. Hardenbergh, J. Catalysis, 87, 66 (1984).

21. H. P. Bonzel, and H. J. Krebs, Surface Sci., 91, 499 (1980).

22. D. L. King and J. B. Peri, Journal of Catalysis, 79, 164 (1983).

23. H. J. Lehmann, M. Ralek, and W. D. Deckwer, Paper No. 133d presented at 73rd Annual Meeting AIChE, Chicago, November (1980).

24. G. C. Maiti, R. Malissa, and M. Baerns, Applied Catalysis, 5, 151 (1983).

25. W. Benecke, H. G. Feller, and M. Ralek, Z. Metallkde., 75(8), 625 (1984).

26. H. Schulz, and H. Gokcebay, H. Proc. Organic React. Soc. Conf., Charleston, SC, April (1982).

27. K. B. Jensen and F. E. Massoth, J. of Catalysis, 92, 98 (1985).

28. K. B. Jensen and F. E. Massoth, J. of Catalysis, 92, 109 (1985).

29. J. Stencel, J. R. Diehl, S. R. Miller, H. W. Pennline, and M. F. Zarochek, Paper presented at 9th North American Meeting of the Catalysis Society, Houston, March 1985.

30. N. V. Sidgwick, "The Chemical Elements and their Compounds," Oxford University Press, New York, NY, 1952.